Desalination and Water Treatment
www.deswater.com

doi: 10.1080/19443994.2016.1179220

57 (2016) 27505–27518
December

Taylor & Francis
Taylor & Francis Group

The improvement of CTA forward osmosis membrane performance by hydrophilic modification on interface between support layer and non-woven fabric

Panpan Guan[a,b], Duo Wang[a,b,*]

[a]*Key Laboratory of Marine Chemistry Theory and Technology, Ministry of Education, Qingdao 266100, China, Tel. +15 224448385; email: 1025707761@qq.com (P. Guan), Tel. +13 805329055; email: wangduo@ouc.edu.cn (D. Wang)*
[b]*College of Chemistry and Chemical Engineering, Ocean University of China, Qingdao 266100, China*

Received 25 September 2015; Accepted 8 April 2016

ABSTRACT

Cellulose triacetate (CTA) forward osmosis (FO) membrane was fabricated with a polyvinyl alcohol (PVA)-modified nonwoven fabric (NWF) as a support material, which helps achieve a significant improvement in membrane performance. First, a surface modification was performed on the NWF by attaching PVA and glutaraldehyde to the fabric by cross-linking. Second, a CTA membrane was cast on the surface of the surface-modified NWF by phase inversion process. Then, the modified NWF and the modified CTA membrane were characterized by infrared spectroscopy, scanning electron microscopy (SEM), and the contact angle. It was found from the infrared spectroscopy that large quantities of hydroxyl group on the surface made the NWF more hydrophilic. It was also found from the SEM that, the PVA was not only attached on the surface of the fabric, but also embedded in the fabric. With the PVA content of the modified CTA membrane increased, the small sponge-like pores in the support layer were changed gradually into bigger finger-like pores. After the PVA modification, the contact angle of the NWF decreased from 116.9° to 38.5°, and that of the modified CTA membrane decreased from 114.1° to 55.8°, leading to a significant improvement in hydrophilicity. As a result, the water flux of the PVA-modified CTA FO membrane in FO mode was greatly improved up to 55 LMH. And the same time the J_s/J_w was only 0.25. It has been calculated that the modified CTA membrane has a porosity of 0.51, and a tortuosity of 0.48, and a structural parameter of 93.65 μm. Compared the PVA-modified CTA membrane with several other FO membranes, it was found that the former has a smaller structural parameter and which can effectively reduce the internal concentration polarization in the support layer, thereby resulting in a significant improvement in membrane performance.

Keywords: Forward osmosis; Cellulose triacetate membrane; NWF; Hydrophilic modification

*Corresponding author.

1. Introduction

With the world's population constantly on the rise and social economy developing nonstop, the strategy employed by any government or social group to achieve peace and development in the future will be closely related to water resources, particularly freshwater ones [1]. As new technologies continue to emerge to reduce the cost of the desalination of seawater, more and more countries turn to membrane desalination to address their water scarcity [2]. Forward osmosis (FO) has been used for the desalination of seawater and brackish water as well as the purification of contaminated water sources [3,4]. FO can be used to dilute the flow of water fed into the desalination unit so as to reduce the energy consumption.

A research group has recently accumulated a huge amount of information on the basic principles and application of FO and revealed that FO may become a highly favorable option for the desalination of water and other forms of wastewater treatment [5]. Due to its many unique advantages, like less energy input [6], lower fouling tendency, easier fouling removal [7,8], and higher water recovery [9], FO has become a promising technology for the production of clean water. During the FO process, the transfer of water through a semi-permeable membrane from a solution under an osmotic pressure to another solution under a higher osmotic pressure occurs due to the osmotic pressure difference of its own accord, and no external energy is required for this form of mass transfer [10]. Over the past decade, FO has been successfully applied to wastewater treatment [11,12], seawater/brackish desalination [13,14], food processing [15,16], pharmaceutical application [17,18], and power generation [19,20].

FO membranes may be prepared using either of the following three major methods [21]: (1) Preparing cellulose membranes through the phase inversion process; (2) the interfacial polymerization preparation of composite membranes; (3) chemical modification of the membrane surface. Among these methods, the phase inversion process is the commonest method for preparing FO membranes.

A typical cellulose triacetate (CTA) FO membrane has an asymmetric structure, which has a dense active rejection layer that is responsible for separation and a porous support layer for better mechanical strength [22–27]. There is a recent rapid surge of interest in research into the CTA membranes for FO and/or pressure retarded osmosis processes that show promising applications in desalination, energy production, and solution concentration [28–31]. Although excellent performance from the CTA membranes was reported in many studies for a short period of time, the membranes still suffered severely from caking, biofouling [32], and chemical instability [33–35], which lead to a rapid decline in membrane performance. Ong et al. [36] studied the fundamentals of engineering and science towards the formation of CTA membranes for FO applications. Zhang et al. [37] studied that membranes with an ultra-thin selective layer and a fully porous support have been fabricated which show high performance in FO processes. Therefore, the ideal support layers for FO membranes to enhance performance would be very thin, highly porous, and provide a direct path from the draw solution to the active surface of the membrane.

However, to reduce the thickness of the support layer, most of the CTA FO membranes were fabricated with polyester mesh as a support material. Although it can effectively reduce the thickness of the membrane and the internal concentration polarization and improve the water flux of the membrane, the strength of the polyester mesh is normally lower than a nonwoven fabric (NWF). Moreover, the polyester mesh may be easily distorted in the membrane process. When making the membranes, the support structure may comprise polyethylene terephthalate or polypropylene (PP) [38].

PP NWF can be used as a support material for the membrane, but it is hydrophobic. Like other common support materials, PP NWF allows limited application due to its hydrophobic properties. Modification is thus needed to improve its water flux. It is well known that polyvinyl alcohol (PVA) can modify the surface of a PP NWF so as to improve the water flux and the rate of rejecting. In the chemical engineering circles there has been thus a great deal of interest in the modification of the NWF surfaces to improve their hydrophilicity and the performance of the membrane.

Surface coating is a usual physical modification method. It uses some chemical properties of the coating material, which forms an ultra-thin hydrophilic coating on the surface without changing the intrinsic properties of the membrane material following the surface modification [39,40].

PVA polymer, with its highly hydrophilic and excellent film-forming properties as well as outstanding physical and chemical stability, is a kind of excellent membrane material for the preparation of a hydrophilic membrane. PVA can be immobilized on the NWF surface by dip-coating, and then a PVA-modified NWF can be formed. A lot of hydroxyl groups on the molecular chain make the PP NWF highly hydrophilic with good film-forming properties and lower resistance to water transportation.

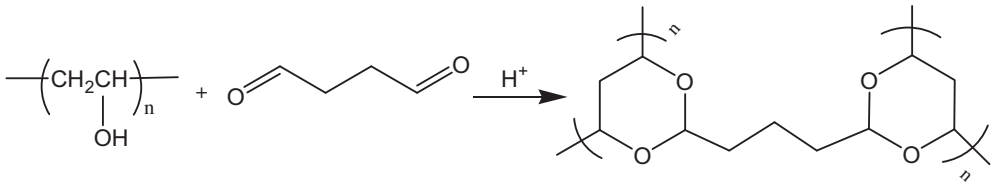

Fig. 1. Mechanism of the cross-linking reaction between PVA and GA on an NWF surface.

Acetylization and cross-linking are common ways to form the PVA membrane. The conventional cross-linking reagent glutaraldehyde (GA) can surface-modifies a lightly cross-linked PVA hydro-gel. The reaction between PVA and GA is between the hydroxyl groups of PVA and the aldhyde to form an acetal bridge, as shown in Fig. 1 [41].

In this paper, we demonstrate the water flux of the modified membrane, which has seen obvious improvement on FO process. Innovative modification of the membrane casting procedure, along with the resultant effects of these changes in the microstructure of the membranes, is described. The structural parameters of the newly modified CTA-FO membranes are compared to those of commercially available FO membranes. These performance results are linked to the membrane structural properties. This paper aims to demonstrate that the interface modifications of the support layer can significantly improve the performance of the CTA membranes, thus providing a basis for further development of osmotically driven membranes.

2. Experiment

2.1. Materials

A fully hydrolyzed PVA powder with a degree of polymerization of 1,700 was obtained from Aladdin Industrial Corporation of Shanghai, China. GA, a cross-linking agent, was obtained as a 50% (w/w) aqueous solution. Methanol, acetic acid, and sulfuric acid were reagent grades and were used without further purification. CTA (Acetyl content: 43–44 wt.%) was purchased from Acros Organics in this work. 1,4-dioxane and acetone were used as the solvents. Methanol and lactic acid were used as additives, whereas pure water and 1 M sodium chloride solution were used as the experimental material and absorbing liquid, respectively.

2.2. Fabrication of CTA FO membrane by phase inversion

2.2.1. Modification of PP NWF

Before the experiment, the PP NWF should be soaked in acetone for 24 h to remove any contamination on the surface of the material. An aqueous PVA solution was prepared by dissolving the polymer in deionized water at 95℃ 2 h. 100 ml of various concentration PVA aqueous solutions were mixed with a cross-linking solution. The cross-linking solution consisted 10 vol.% sulfuric acid, 10 vol.% acetic acid, and 10 vol.% methanol according to a volume ratio of 1:2:3, with an appropriate amount of GA thrown in as well. The NWF was quickly immersed in the cross-linking solution before being placed in a shaking incubator with a shaking speed of 150 rpm at 50℃ for 1 h to facilitate the cross-linking reaction. After that, the PVA-modified NWF was allowed to dry at 70℃ for 1 h in an oven and placed in deionized water for 24 h to remove any residual cross-linking agent, PVA, etc.

2.2.2. The preparation of cellulose acetate membranes

Polymer solutions were prepared by dissolving CTA (13.9 wt.%) in a mixed solvent of acetone (18.4 wt.%) and 1, 4-dioxane (53.2 wt.%). Methanol (8.2 wt.%) and lactic acid (6.3 wt.%) were additives, which were stirred until total dissolution at room temperature before being left to stand until complete deaeration. Under the condition of a certain temperature (20℃) and humidity (above 90%), solutions were then cast on an unmodified or hydrophilic-modified PP NWF with a casting knife, followed by immersion in a tap water bath at 25℃,1 h. After the removal of residual solvents, membranes underwent heat treatment 60℃, 10 min. Finally, the membranes were stored in a sodium-bisulfite solution (1 mol/L).

2.3. Membrane tests in FO

A schematic diagram of an advanced bench-scale FO membrane test apparatus is illustrated in Fig. 2. The simplest apparatus for the testing of FO membranes comprises a FO membrane cell, two low-pressure recirculation pumps (one for the feed and the other the draw solution. The raw material liquid is deionized water, and the drawing liquid is 1 mol/L NaCl solution. The test was conducted at room

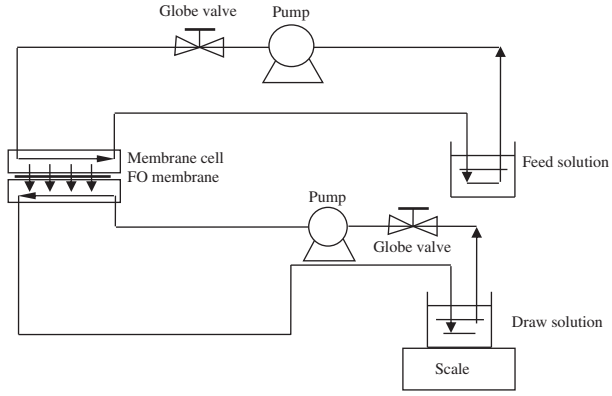

Fig. 2. Schematic diagram of the laboratory-scale FO system.

temperature), feed and draw solution tanks, and a hydraulic system of pipes, tubes, connectors, and valves. The materials of all the wetted parts should be corrosion resistant (plastic or stainless steel). The membrane cell usually comprises two flow channels of the same dimensions, one on each side of the membrane.

During the experiment, the raw material and drawing liquid in the peristaltic pump flowed on both sides of the membrane test pool, in the form of cross-flow flow. The drawing liquid side is connected to the electronic balance to measure the quality of the raw material liquid side change, and to calculate the water flux of the membrane using electrical conductivity meter measuring absorption of the solute in liquid conductivity. FO mode was used to measure the performance of the CTA membrane, namely the density of the membrane is toward feed solution and the porous support layer is toward draw solution.

2.3.1. Water flux (J_w)

Water flux of the membrane refers to the volume of water going through the membrane in unit time per unit area. The unit commonly used is LMH (L m^{-2} h^{-1}).

$$J_w = \frac{\Delta W}{\rho w \times A \times t} \quad (1)$$

where ΔW (g) is the water quantity through the area of A (m^2) within t (h). ρw is the density of water (1000 g m^{-3}).

2.3.2. Reverse salt flux J_s

Reverse salt flux of the membrane refers to the amount of salt transferred through the membrane from draw to feed solution in a period of time. The unit commonly used is LMH (g m^{-2} h^{-1}).

$$J_s = \frac{(C_t V_t - C_0 V_0)}{A \times t} \quad (2)$$

where C_t and C_0 is the concentration of salt in the feed at the t time and the start of experiment, respectively. V_t and V_0 is the volume of the feed solution at the t time and the start of experiment, respectively. The parameter A and t is membrane surface area and the measurement time, respectively.

$$\frac{J_s}{J_w}$$

J_s/J_w of the membrane reflects the interception capacity of the membrane. J_s/J_w relates the water flux, J_w, and reverse salt flux, J_s. The unit commonly used is LMH (g/L).

2.4. Determination of the membrane characteristic parameters

The intrinsic water permeability coefficient (expressed as A) and salt permeability coefficient (expressed as B) of the membrane were characterized in the RO test apparatus, according to the procedure described in an earlier study [42]. The pure water permeability A and salt rejection were tested at room temperature with the denser layer facing the feed. The pure permeability measurements were conducted with distilled water and transmembrane pressure of 5.0 bar. To measure salt rejection, 200 ppm NaCl solution was used and the trans-membrane pressure was 5.0 bar. The concentrations of NaCl in the feed (C_f) and permeate (C_p) were determined by conductivity measurements. R was calculated according to Eq. (2):

$$R = 1 - \frac{C_p}{C_f} \quad (3)$$

B was determined by a linear fitting based on Eq. (3) [22]:

$$B = J_w \left(\frac{1-R}{R}\right) \exp\left(-\frac{J_w}{k}\right) \quad (4)$$

where k is the mass transfer coefficient for the cross-flow channel of the RO membrane cell.

A was determined by Eq. (4):

$$A = \frac{J_w}{\Delta P} \tag{5}$$

where Δp is the hydraulic pressure applied.

2.5. Porosity ξ

For the measurement of porosity, wet membranes were taken out from the water bath. Then the excess water was removed using tissue paper. The membrane was then weighed (m_1, g). Then the membrane was dried in a vacuum drying oven, and re-weighed (m_2, g). The density of water is ρ_w (1.00 g/cm^3) and the density of CTA is ρ_{CTA} (1.31 g/cm^3). The porosity ξ is then obtained:

$$\xi = \frac{(m_1 - m_2)/\rho_w}{(m_1 - m_2)/\rho_w + m_2/\rho_{CTA}} \times 100 \tag{6}$$

2.6. Structural parameter S_t

The water flux in the PRO mode shows a better performance than that in the FO mode, which is attributed to the severer ICP of the latter, as to be discussed in the following. Dilutive ECP occurs when the draw solution is placed against the selective layer in the PRO mode, and the osmotic pressure at the membrane surface $\pi_{D,m}$ can be obtained with the following equation:

$$\pi_{D,m} = \pi_{D,b} \exp\left(-\frac{J_w}{k}\right) \tag{7}$$

where J_w is the experimental water flux, k is the mass transfer coefficient, and $\pi_{D,b}$ is the bulk osmotic pressure of the draw solution.

On the contrary, when the feed solution is facing against the selective layer in the FO mode, concentrative ECP would happen which gives the osmotic pressure at the membrane surface $\pi_{F,m}$ by:

$$\pi_{F,m} = \pi_{F,b} \exp\left(\frac{J_w}{k}\right) \tag{8}$$

where $\pi_{F,b}$ is the bulk feed osmotic pressure. The mass transfer coefficient, k, can be calculated by the following equation [43]:

$$k = \frac{ShD_s}{d_h} \tag{9}$$

where D_s is the solute diffusion coefficient, d_h is the hydraulic diameter, and Sh is the Sherwood number of a laminar flow in a rectangular channel given by:

$$Sh = 1.85\left(\mathrm{Re}\ \mathrm{Sc}\frac{d_h}{L}\right)^{0.33} \tag{10}$$

Here, Re is the Reynolds number, Sc is the Schmidt number, and L is the length of the channel. Lee et al. has developed the following expression to model the flux under ICP in the PRO application:

$$J_w = \frac{1}{K}\ln\frac{A\pi_{D,b} + B}{A\pi_{F,m} + B + J_w} \tag{11}$$

$$S_t = \frac{D_s}{J_w}\ln\frac{A\pi_{D,b} + B}{A\pi_{F,m} + B + J_w} \tag{12}$$

The water flux, J_w, using a 1 M NaCl draw solution and deionized water feed solution was measured with the membrane in FO mode (i.e. active layer facing the feed solution). The membrane support structural parameter was determined using.

Here, K is the solute resistivity for diffusion within the porous layer given by:

$$K = \frac{S_t}{D_s} \tag{13}$$

where S_t is the structural parameter of the membrane defined by tortuosity, τ, porous layer thickness, t, and porosity, ε.

$$S_t = \frac{\tau t}{\varepsilon} \tag{14}$$

2.7. Characterization

2.7.1 FTIR-ATR

To investigate the chemical changes of the PVA-modified and the original NWF surfaces, the surface analyses were performed by using Fourier transform spectroscopy infrared with attenuated total reflection (FTIR-ATR). The FTIR/ATR spectra of the PVA-modified and the original NWF were measured by a Nicolet IS 10 instrument (Thermo Scientific Nicolet, USA). Prior to the measurements, the samples were dried in a vacuum chamber at 75°C for 24 h.

2.7.2. Scanning electron microscopy (SEM)

Cross-sectional and topographical phase morphologies of the PVA-modified and original NWF were inspected by scanning electron micrograph (SEM) using a Hitachi S-4800 scanning microscope. The NWFs which were dried at room temperature were kept in liquid nitrogen and fractured. All samples were coated with a thin gold layer using sputter coater.

2.7.3. Contact angle

The static contact angles of the PVA-modified and the original NWF were measured to quantify the change in hydrophilicity using an optical contact angle measuring system OCA20 (Data Physics Instruments GmbH, Germany). An ultra-pure water drop (10 μL) was added to a dry sample in an ambient atmosphere and humidity by a micro-syringe, which was then observed through a traveling microscope fitted with a goniometer eyepiece. The data shown represent an average of over five measurements performed on five different areas of the same sample.

3. Results and discussion

3.1. Effects of PVA on NWF properties

3.1.1. Characterization of the modified NWFs by ATR-FTIR

Surface hydrophilicity was determined by changes in the chemical element and composition of the NWF surface. Here, we investigated the topography and followed the chemical changes of PVA-modified and original NWF surfaces to uncover the origin of the hydrophilic-modified surface. Fig. 3 compares the IR spectra of modified NWF (graphs b, c) with that of an unmodified NWF (graph a).

After PVA modification, a thin hydro-gel layer of PVA was created on the surface of the NWF, which could be confirmed by an FTIR/ATR spectroscopy analysis. In graph (a), the peaks observed at 2,917 and 2,850 cm^{-1} correspond to the symmetric and asymmetric stretching vibration of C–H; the peaks observed at 1,376–1,457 cm^{-1} correspond to the symmetric and asymmetric bending vibration of C–H. Comparing the PVA-GA cross-linking-modified NWF (graph b) to the unmodified NWF (graph a), the three new absorption peaks are shown in graph (b). The absorption peak at about 1,135 cm^{-1} for the C–O–C group can be attributed to the formation of an acetal ring and ether linkage as a result of the reaction between the hydroxyl groups of PVA and GA at the NWF surface. The

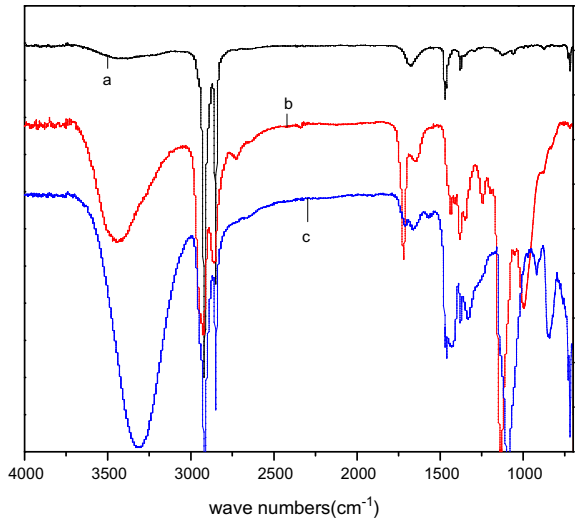

Fig. 3. FTIR-ATR spectra of NWF (a) unmodified, (b) PVA-GA modified, and (c) PVA modified.

absorption peak at about 1,720 cm^{-1} for the carbonyl group can be attributed to ester carbonyl group formed from the esterification reaction between PVA and acetic acid. The distinct broad absorption peak at about 3,445 cm^{-1} is for the OH group, which was due to the stretch of the hydrogen bond with OH group. Comparing the PVA-modified NWF (graph c) to the unmodified NWF (graph a), the only new absorption peak is shown in graph (c). The distinct absorption band at about 3,340 cm^{-1} was due to the stretching vibration of OH group of PVA, but the PVA is easily lost. The GA-PVA cross-linking modification is therefore not easy to lose compare to only PVA modification.

3.1.2. Surface properties of the NWFs and CTA membranes (water contact angle)

The measurement of the contact angle between ultra-pure water and an NWF surface is one of the easiest ways to characterize the hydrophilicity of NWF surface. When water is applied to the surface, the outermost surface layers interact with the water. A hydrophobic surface with low energy gives a high contact angle with water, whereas a wet high-energy surface allows the drop to spread, i.e. gives a low contact angle [44]. Such changes in hydrophilicity are reflected in contact angles of such modified NWFs and CTA membranes. The contact angle data were collected for PVA-modified NWF as well as CTA membrane (as shown in Table 1) and the results are shown in Figs. 4 and 5.

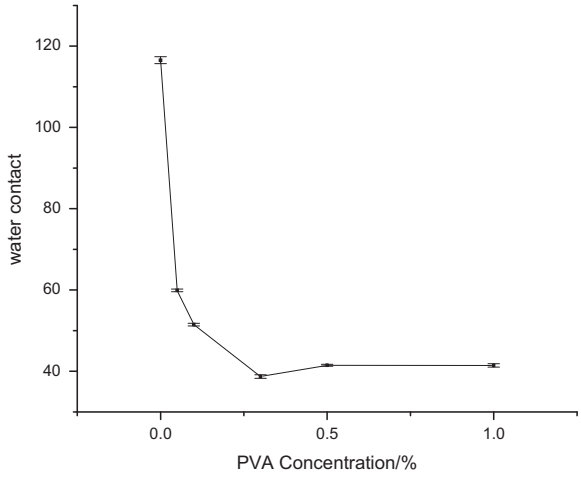

Fig. 4. Changes in contact angle of NWF surface with PVA concentration.

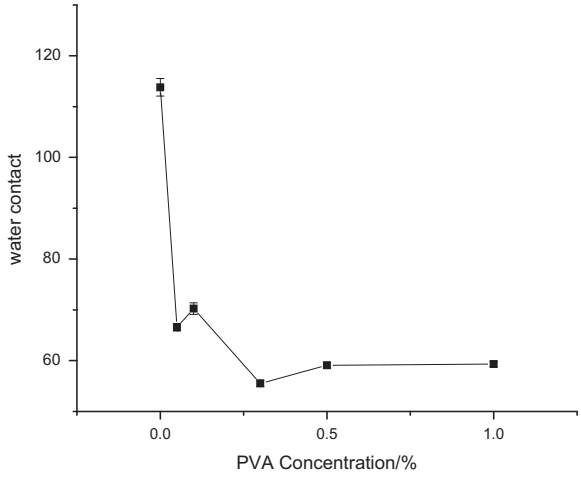

Fig. 5. Changes in contact angle of CA membrane-modified surface with PVA concentration.

Fig. 4 depicts the variant dependence of static contact angle (SCA) of the PVA-modified NWF at the concentration of 0, 0.05, 0.1, 0.3, 0.5, and 1.0 wt.% PVA. The plot indicates the SCA of the samples underwent a significant change. For the unmodified NWF, the surface is strongly hydrophobic and the measured water contact angle was 117˚. However, after surface modification, the water contact angle declines gradually to 42˚ with the increase of PVA concentration. This means the NWF surface is somewhat hydrophilic after the immobilization of PVA. Therefore, the hydrophilicity increase for the NWF mentioned above is mainly due to the PVA hydro-gel immobilized on the NWF surface.

Fig. 5 depicts that the contact angle of the modified FO membrane and that of the modified NWF are consistent. With the increase in PVA concentration, the water contact angle becomes smaller. The size of the contact angle is mainly determined by the modified support material layer. Since the thin separation layer is about 5–10 μm, and more hydrophilic nonwoven makes it easier for water infiltration. Water contact angle therefore decreases with the increase in PVA concentration.

3.1.3. Scanning electron microscopy (SEM)

Firstly, SEM was employed to examine the surface and the cross-section structure of PVA-modified NWF. The SEM pictures show the NWF surface became smoother by cross-linking with PVA (Fig. 6(d)) compared with the micrograph of the unmodified NWF (Fig. 6(e)). It is also seen that the surface porosity was somewhat reduced because the PVA hydro-gel covered the unmodified surfaces of the NWF. The surface of the PVA-modified NWF is shown in Fig. 6(c). In comparison with the micrograph of the unmodified NWF (Fig. 6(a)), it is obvious that modified NWF is denser and smoother. Fig. 6(a), (b), and (c) shows the top surface of the modified NWF. With the increased concentration of the PVA, the SEM pictures show that the NWF surface became smoother by cross-linking with PVA. As a result, more O–H is absorbed on the surface of the NWF surface. The hydrophilic of the modified NWF are significantly improved. Fig. 6(b) shows the cross section of the modified NWF. It can be seen that the circumferences of the NWF are coated with PVA and the void space between the fibers is reduced. Coverage of the void space may be continuous when the fibers are closely packed. Not only PVA–GA covered the surface of the NFW, but also it impregnated in pores of NWF. The NWFs were modified, which means the surface of the NWF is somewhat hydrophilic.

Several experiments were conducted to study the effect of PVA modification on the structures of the membranes. It can be seen from the scanning electron micrograph of membrane surface (Fig. 7) that the surface of cross-linking PVA-modified CAT membrane is smooth and flat. A very thin top surface layer was also observed in Fig. 8. With the increase in the concentration of PVA, more pores were seen in Fig. 8. Fig. 8 showed that with the increase of the concentration of PVA, the pore structure of the support-layer gradually changed from sponge-like pore to bigger finger-like pore structure.

The cross-section of PVA-modified CTA membrane was investigated as shown in Fig. 8. A very thin top

Table 1
Contact angles of the NWFs and CTA membranes

Species	Contact angle of NWFs (°)	Contact angle of CTA membranes (°)
Unmodified	116.5 ± 0.8	113.8 ± 1.7
0.05 wt.% PVA modified	59.9 ± 0.3	66.5 ± 0.7
0.1 wt.% PVA modified	51.5 ± 0.3	70.2 ± 1.1
0.3 wt.% PVA modified	38.7 ± 0.4	55.5 ± 0.6
0.5 wt.% PVA modified	41.5 ± 0.2	59.1 ± 0.5
1.0 wt.% PVA modified	41.4 ± 0.4	59.3 ± 0.5

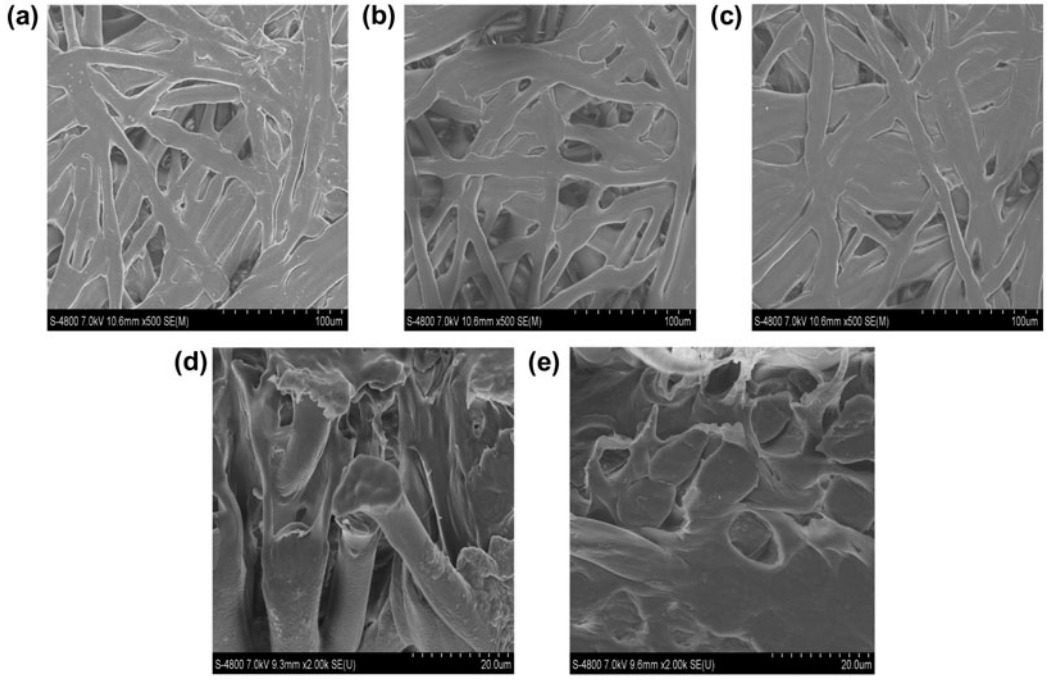

Fig. 6. The top surface of PVA-modified NWF made from varying the concentration of PVA (a) PVA: 0 wt.%, (b) PVA: 0.1 wt.%, (c) PVA 0.3 wt.%, magnified × 500, (d) Scanning electron micrograph of the cross section of the unmodified NWF magnified × 2.0 k, PVA: 0 wt.%, and (e) Scanning electron micrograph of the cross section of the PVA-modified NWF magnified × 2.0 k, PVA: 0.3 wt.%.

surface layer was also observed in Fig. 8(b). The SEM images of Fig. 8(c)–(f) showed that with the increase in PVA concentration, the pore structure of the support layer was changed gradually from sponge-like pores to bigger finger-like pores, which significantly made the water flux increasing.

3.2. Parameters of modified CTA membranes

The performance of FO membrane is characterized by FO water flux, reverse salt flux, J_s/J_w, as well as the water flux and retention rate in case of reverse osmosis. In FO tests, when the separation layer of membrane faces the side of raw material liquid, it is FO mode; when the separation layer of membrane faces the side of absorbing liquid, it is PRO mode. Figs. 9a–9c are relevant schematic diagrams showing the changes of water flux, reverse salt flux and J_s/J_w along with the changes of PVA content under FO and PRO mode of PVA-modified CTA membranes, respectively. It could be seen from the figures that, under PRO mode, PVA-modified CTA membrane has higher

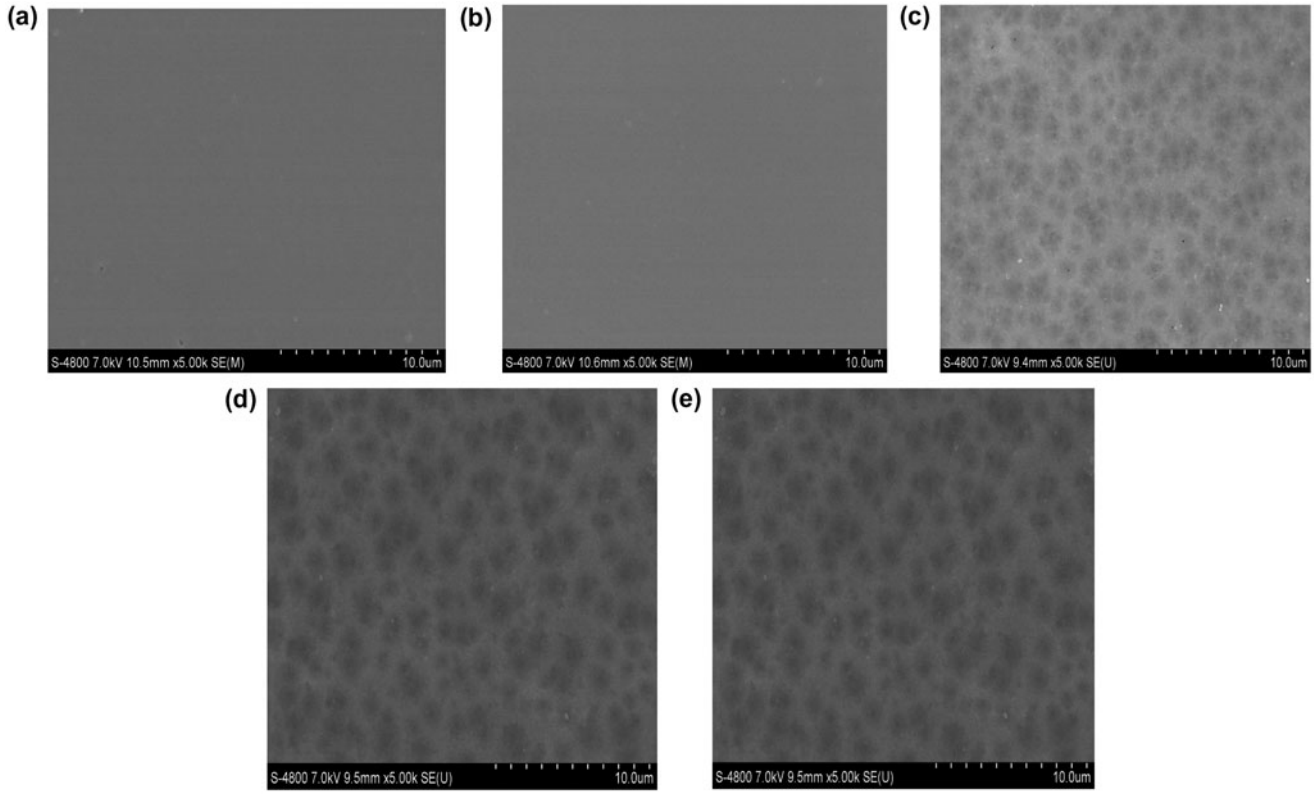

Fig. 7. The top surface of PVA-modified CTA membranes made from varying the concentration of PVA: (a) PVA: 0 wt.%, (b) PVA: 0.05 wt.%, (c) PVA: 0.1 wt.% PVA, (d) PVA: 0.3 wt.%, and (e) PVA: 0.5 wt.%, magnified × 5.00 k.

water flux, lower reverse salt flux and relatively low J_s/J_w. Under FO mode, diluted concentration polarization occurs, while diluted internal concentration polarization has greater influences on water flux than concentrated internal concentration polarization. So water flux is relatively low. The direction of solvent diffusion is opposite to that of water permeation, and under PRO mode, for relatively high water flux, the resistance for reverse diffusion of NaCl is relatively big, and the reverse salt diffusion flux is relatively low.

The research surveys the influence of the PVA content on the performance of FO membrane. It could be seen from the figure that, PVA-modified membrane has a greatly raised water flux, and an obviously lowered reverse salt flux. Along with the increase in PVA content, the performance of PVA-modified membrane presents the trend of "rise first and drop then." This is related to the improved hydrophilicity of membrane brought by PVA modification, and its trend is accordant with the change trend of membrane contact angle (Figs. 3 and 4). The performance of the PVA-modified CTA membrane was improved when the pore of the PVA-modified CTA membrane changed from sponge-like pore to big finger-like pore structure (Figs. 7 and 8). These results corresponded well with the structural characteristics of the membranes and their substrate as discussed in last sections.

Figs. 9a and 9b depicts the dependence of the FO water flux, the PRO water flux and Js/Jw on the concentrations of 0, 0.05, 0.1, 0.3, and 0.5 wt.% PVA. (1 M NaCl as draw solution in FO and PRO mode). With the increased concentration of PVA, the water flux first increases before decreasing. Meanwhile, the reverse salt flux first decreases before increasing. With the increase in PVA concentrations from 0 to 0.3 wt.%, the amount of immobilization degree of PVA on NWF surface was increased gradually (Fig. 6), leading to an increase in the water flux with increasing PVA concentration. Interestingly, the increase in water flux at the concentration of 0.3 wt.% PVA was more noticeable than those of 0.05 and 0.1 wt.%. However,

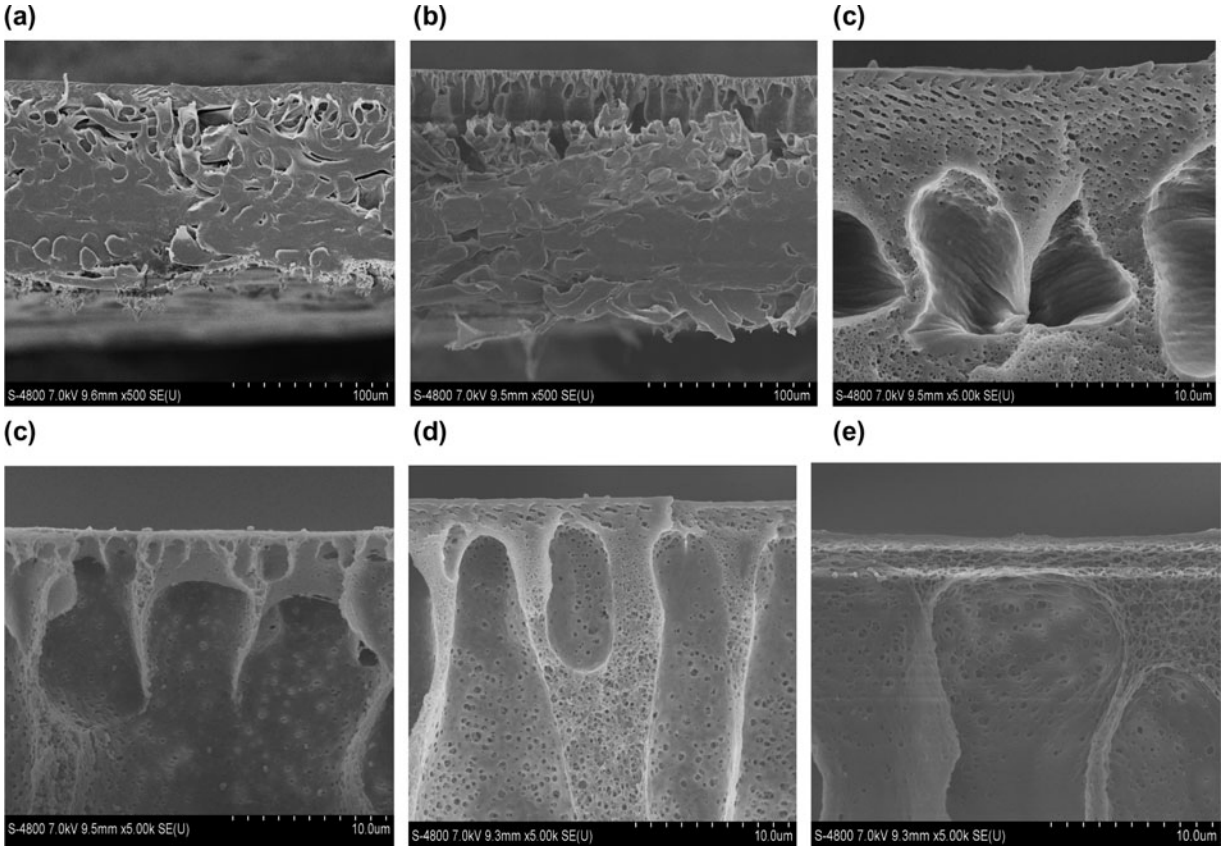

Fig. 8. (a) Scanning electron micrograph of the cross section of the unmodified CTA membrane, magnified × 500, (b) Scanning electron micrograph of the cross section of the 0.3 wt.% PVA-modified CTA membrane, magnified × 500; The cross section of PVA-modified CTA membranes made from varied the concentration of PVA, (c) PVA: 0.05 wt.%, (d) PVA: 0.1 wt.%, (e) PVA: 0.3 wt.% PVA, and (f) PVA: 0.5 wt.%, magnified × 5.00 k.

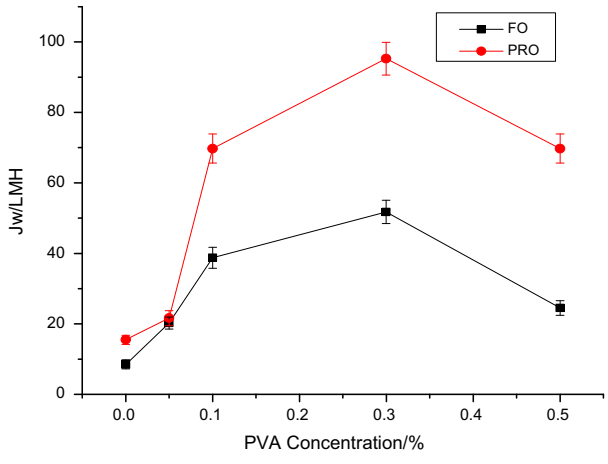

Fig. 9a. Variation of CTA membrane water flux with PVA concentration.

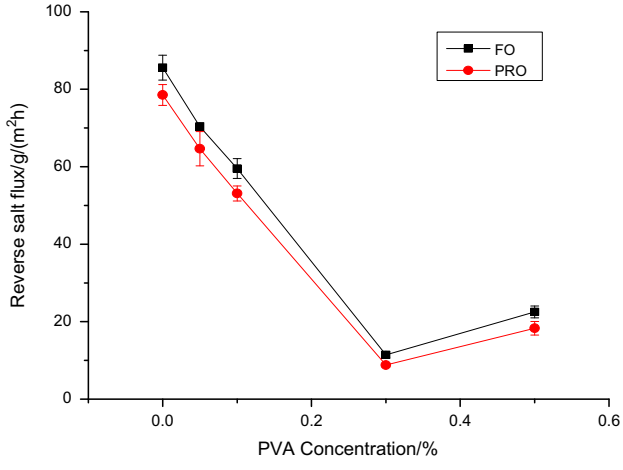

Fig. 9b. Variation of CTA membrane reverse salt flux with PVA concentration.

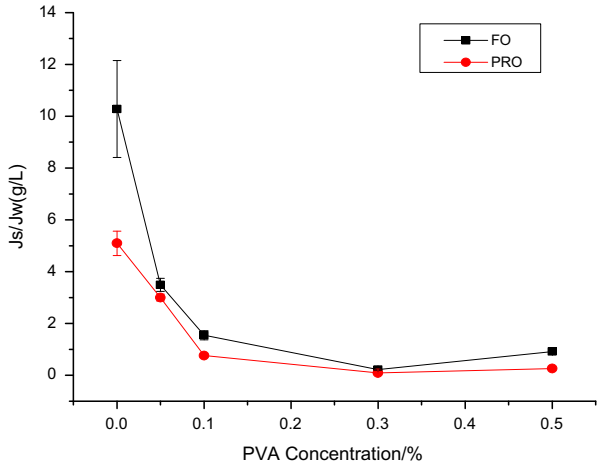

Fig. 9c. Variation of CTA membrane J_s/J_w with PVA concentration.

the water flux was decreased a little at PVA concentration between 0.3 and 0.5 wt.%. These observations might be attributed to the cross-linked degree of PVA and GA. Cross-link of PVA and GA forms hydro-gel matrix. When quality fraction of PVA is too small, cross-linked degree is small, and hydro-gel matrix is relaxed. Water is not contained easily. However, when quality fraction of PVA is higher, cross-linked degree is also higher. There may be some crystal domain formation in the hydro-gel matrix, which results in the smaller space of hydro-gel matrix. This implies that the osmotic permeability of PVA-modified membrane is significantly influenced by the pore structure and wettability of the substrate, which are related to the concentration of PVA. More open macro voids and wettability of membrane substrate layer is beneficial to reduce mass transfer resistance in the FO process. These results corresponded well with the structural characteristics of the membranes and their substrate as discussed in last sections. First, from SEM, with the increased concentration of PVA, the structure of the pores changes from spongy pore structure to finger-sized holes. 0.3 wt.% PVA-modified CTA membrane has the largest finger-sized pores, the highest number of pores in the membrane. Second, from the water contact angle, with the increased concentration of PVA, the contact angle decreases gradually. The 0.3 wt.% PVA-modified CTA membrane has the smallest water contact angle. Fig. 9b shows the reverse salt flux among the membranes. The 0.3 wt.% PVA-modified membranes showed the lowest reverse salt flux, indicating an active top layer formed in the membrane was dense and homogeneous without leakage.

Feed solution: deionized water; draw solution: 1 M NaCl; liner flow rate: 2.4 cm/s; temperature: 25℃.

To quantify the effect of the structure of modified substrate on the FO performance and understand the contribution of the active layer and substrate layer to the permeability, illustration may be done based on membrane performance parameters. The water and solute permeability coefficients (A and B) and structure parameter (S_t) as well as the ratio of tortuosity (τ) to porosity (ξ) of the membranes were calculated from the RO experimental data, and the results are presented in Table 2. Adding an appropriate amount of PVA to the casting solution improved the performance of the modified CTA membrane. The addition of a small amount of PVA (0.05–0.1 wt.%) led to slightly reduced structural parameter, whereas the addition of PVA (0.1–0.3 wt.%) significantly decreased the tortuosity of substrate pores, while porosity increased as shown in Table 2. This resulted in a higher permeability of membrane but at the expense of selectivity. PVA has a positive effect on the permeability of the substrate, indicating that the hydraulic resistance of the FO membrane would decrease. The pure water permeability (A) was significantly improved, following the increase of the PVA loading from 0 to 0.5 wt.%. However, higher concentration of PVA (0.5 wt.%) only leads to a slight improvement in the pure water permeability (A). When the concentration of PVA is 0.3 wt.%, A is the highest and B has the smallest value. Therefore, the significant change in water permeate flux may be due to the increase in porosity and the decrease in tortuosity as can be confirmed through the SEM. Fig. 8 shows the SEM images of the cross sections of the PVA-modified membrane. It indicates that all substrates show a typical asymmetrical structure consisting of a skin layer.

3.3. The contrast between the different membrane parameters

Unmodified CTA membrane has a rather high A value, and even though the membrane is of relatively small thickness, its S_t is still relatively big thanks to the support of NWF; as for the CTA membrane modified with PVA (0.3 wt.%), modification makes the A of membrane increased obviously and even higher than that of TFC-FO membrane, and meanwhile, it makes S_t lowered obviously, indicating that modified membrane has smaller internal concentration polarization, and so, has better performance in permeating process.

A comparison of membrane performance and structural parameters in this paper with other membranes published in literature is listed in Table 3.

Table 2
Summary of calculated intrinsic separation properties and structural parameters of different PVA-modified CTA membranes

PVA concentration (%)	RO model J_w	RO model R	FO model J_w	Water permeability A (LMH bar^{-1})	NaCl permeability B (LMH)	Membrane thickness (μm)	Porosity (%)	Tortuosity	Structural parameter S_t (μm)
0	8.2	0.97	10.0	1.64	0.222	90	35.04	5.1348	1,318.86
0.05	11.0	0.965	22.5	2.20	0.335	92	46.49	2.0700	409.98
0.1	12.3	0.983	40.0	2.46	0.175	96	49.96	0.8425	161.89
0.3	13.5	0.95	55.0	2.70	0.573	101	51.38	0.4764	93.65
0.5	13.0	0.972	25.0	2.60	0.304	106	48.75	1.7441	379.24

Notes: FO mode: feed solution: Deionized water; draw solution: 1 M NaCl.
RO mode: When measuring the pure water flux, feed solution: Deionized water; when measuring the rejection, feed solution: 200 ppm NaCl. ΔP is 5 bar. The linear velocity is 2.4 cm/s.

Table 3
FO performance and structural parameters of different membranes

Membrane	Water permeability A (LMH bar^{-1})	NaCl permeability B (LMH)	Membrane thickness (μm)	Structural parameter S_t (μm)	Refs.
PVA (0.3%)-modified CTA membrane	2.70	0.573	110	93.65	This work
HTI membrane	0.67	0.400	–	678.00	[45]
TFC membrane	2.56	0.400	–	670.00	[19]
CA membrane	0.72	0.220	~250	2,500.00	[19]
Unmodified CTA membrane	1.64	0.222	95	1,318.86	This work

In comparison with the CTA membrane, it is obvious the unmodified CTA membrane has bigger A, smaller membrane thickness and smaller S_t. But in comparison with the unmodified CTA membrane, it is evident that the modified CTA membrane has bigger A and B, a slightly thicker membrane and much smaller S_t. The PVA (0.3 wt.%)-modified CTA membrane has bigger A and B, but the S_t is the smallest compared with the HTI membrane. In comparison with the PVA (0.3 wt.%)-modified CTA membrane and the TFC membrane, it is obvious the PVA (0.3 wt.%)-modified CTA membrane has similar A and B and smaller S_t. Obviously, our membrane possesses much lower S_t value than others. The effective modification of PVA reduces the S_t value of the membrane performance, thereby reducing the ICP and gets a better CTA membrane.

4. Conclusion

The data presented in this paper demonstrate that PVA has a significant effect on the flux behavior of the FO process. The propylene NWF was modified by PVA, then CTA membrane was prepared through phase conversion using a modified NWF as a support material. Through infrared analysis, hydroxyl groups were found on the surface of NWF. SEM characteristics show that, the adding of PVA makes the pore structure of membrane support layer change from sponge to bigger finger structure. Contact angle characteristics show that, the contact angle of both modified NWF and modified CTA membrane is obviously reduced, indicating that their hydrophilicity is improved. The performance test of FO membrane shows that modified CTA membrane has obviously improved water flux, and also smaller relative salt values (J_s/J_w). The calculation shows that, modified CTA FO membrane has an increased porosity (ξ), obviously decreased pore tortuosity parameter (τ), and an obviously lowered structure parameter (S_t). This is because that, the interface between FO membrane support layer and NWF, through modification with PVA, has better hydrophilicity, makes the exchange of solvent and water easier during membrane formation, brings about instantaneous phase conversion during formation of support layer, and increases the proportion of

finger pores. Meanwhile, the improvement of interface hydrophilicity reduces water transmission resistance, and raises the water flux of final membrane.

This PVA-modified membrane outperformed the commercial HTI membranes and among others in terms of minimizing the structural parameter which is the direct indicator of internal concentration polarization. Our modified CTA membrane has shown lower S_t parameter compared to other membranes previously fabricated. Thus, modification of FO membranes with PVA is a promising approach for high performance FO membrane development.

References

[1] G. Congjie, G. Genjiang, W. Meng, W. Duo, G. Xueli, Z. Yong, Forward Osmosis: A new way of water purification and desalination, Water Treat. Technol. 34 (2008) 1–5.

[2] K. Kranhold, Available from: <http://online.wsj.com/article/SB120053698876396483.html?mod=googlenews_wsj>.

[3] R.A.L. Jones, A.J. Ryan, H. Storey, M. Butler, C.J. Crook, Apparatus and method for purifying water by forward osmosis, WO2008059219, 2008.

[4] R. McGinnis, Osmotic desalination process, US2005145568 A1, 2005.

[5] T.Y. Cath, A.E. Childress, M. Elimelech, Forward osmosis: Principles, applications, and recent developments, J. Membr. Sci. 281 (2006) 70–87.

[6] R.L. McGinnis, M. Elimelech, Energy requirements of ammonia–carbon dioxide forward osmosis desalination, Desalination 207 (2007) 370–382.

[7] E.R. Cornelissen, D. Harmsen, K.F. de Korte, Q. Jian-Jun, H. Oo, L.P. Wessels, Membrane fouling and process performance of forward osmosis membranes on activated sludge, J. Membr. Sci. 319 (2008) 158–168.

[8] M. Baoxia, M. Elimelech, Organic fouling of forward osmosis membranes: Fouling reversibility and cleaning without chemical reagents, J. Membr. Sci. 348 (2010) 337–345.

[9] C.R. Martinetti, A.E. Childress, T.Y. Cath, High recovery of concentrated RO brines using forward osmosis and membrane distillation, J. Membr. Sci. 331 (2009) 31–39.

[10] W.Y. Kai, T.-S. Yu, G. Chung, Amy, developing thin-film-composite forward osmosis membranes based on the PES/SPSf substrate through interfacial polymerization, AIChE J. 58 (2011) 770–781.

[11] E.R. Cornelissen, D. Harmsen, E.F. Beerendonk, Q. Jian-Jun, H. Oo, K.F. de Korte, J.W.M.N. Kappelhof, The innovative osmotic membrane bioreactor (OMBR) for reuse of wastewater, Water Sci. Technol. 63 (2011) 1557–1565.

[12] R.E. Kravath, J.A. Davis, Desalination of sea water by direct osmosis, Desalination 16 (1975) 151–155.

[13] J.R. McCutcheon, R.L. McGinnis, M. Elimelech, A novel ammonia–carbon dioxide forward (direct) osmosis desalination process, Desalination 174 (2005) 1–11.

[14] K.B. Petrotos, P.C. Quantick, H. Petropakis, Direct osmotic concentration of tomato juice in tubular membrane—Module configuration. II. The effect of using clarified tomato juice on the process parameters on the process performance, J. Membr. Sci. 160 (1999) 171–177.

[15] K.B. Petrotos, H.N. Lazarides, Osmotic concentration of liquid foods, J. Food Eng. 49 (2001) 201–206.

[16] G. Santus, R.W. Baker, Osmotic drug delivery: A review of the patent literature, J. Controlled Release 35 (1995) 1–21.

[17] K.Y. Wang, M.M. Teoh, A. Nugroho, T.S. Chung, Integrated forward osmosis membrane distillation (FO–MD) hybrid system for the concentration of protein solutions, Chem. Eng. Sci. 66 (2011) 2421–2430.

[18] S. Loeb, Production of energy from concentrated brines by pressure-retarded osmosis: I. Preliminary technical land economic correlations, J. Membr. Sci. 1 (1976) 49–63.

[19] T. Thorsen, T. Holt, The potential for power production from salinity gradients by pressure retarded osmosis, J. Membr. Sci. 335 (2009) 103–110.

[20] G. Qingchun, S. Jincai, T.-S. Chung, G. Amy, Hydrophilic superparamagnetic nanoparticles: Synthesis, characterization and performance in forward osmosis processes, Ind. Eng. Chem. Res. 50 (2010) 382–388.

[21] Z. Shuaifei, Z. Linda, C.Y. Tang, D. Mulcahy, Recent developments in forward osmosis: Opportunities and challenges, J. Membr. Sci. 396 (2012) 1–21.

[22] S. Loeb, L. Titelman, E. Korngold, Effect of porous support fabric on osmosis through a Loeb-Sourirajan type asymmetric membrane, J. Membr. Sci. 129 (1997) 243–249.

[23] W. Yining, F. Wicaksana, C.Y. Tang, A.G. Fane, Direct microscopic observation of forward osmosis membrane fouling, Environ. Sci. Technol. 44 (2010) 7102–7109.

[24] W. Rong, S. Lei, C.Y. Tang, C. Shuren, Q. Changquan, A.G. Fane, Characterization of novel forward osmosis hollow fiber membranes, J. Membr. Sci. 355 (2010) 158–167.

[25] C. Shuren, S. Lei, W. Rong, C.Y. Tang, Q. Changquan, A.G. Fane, Characteristics and potential applications of a novel forward osmosis hollow fiber membrane, Desalination 261 (2010) 365–372.

[26] N.Y. Yip, A. Tiraferri, W.A. Phillip, J.D. Schiffman, M. Elimelech, High performance thin-film composite forward osmosis membrane, Environ. Sci. Technol. 44 (2010) 3812–3818.

[27] W.Y. Kai, T.-S. Chung, Q. Jian-Jun, Polybenzimidazole (PBI) nanofiltration hollow fiber membranes applied in forward osmosis process, J. Membr. Sci. 300 (2007) 6–12.

[28] B.D. Coday, D.M. Heil, X. Pei, T.Y. Cath, Effects of transmembrane hydraulic pressure on performance of forward osmosis membranes, Environ. Sci. Technol. 47 (2013) 2386–2393.

[29] A. Achilli, T.Y. Cath, A.E. Childress, Power generation with pressure retarded osmosis: An experimental and theoretical investigation, J. Membr. Sci. 343 (2009) 42–52.

[30] G. Yangshuo, W. Yi-Ning, W. Jing, C.Y. Tang, Organic fouling of thin-film composite polyamide and cellulose triacetate forward osmosis membranes by oppositely charged macromolecules, Water Res. 47 (2013) 1867–1874.

[31] T.P.N. Nguyen, E.T. Yun, I.C. Kim, Y.N. Kwon, Preparation of cellulose triacetate/cellulose acetate (CTA/CA)-based membranes for forward osmosis, J. Membr. Sci. 433 (2013) 49–59.

[32] S. Ebrahim, M. Abdel-Jawad, Economics of seawater desalination by reverse osmosis, Desalination 99 (1994) 39–55.
[33] R. Shukla, M. Cheryan, Stability and performance of ultrafiltration membranes in aqueous ethanol, Sep. Sci. Technol. 38 (2003) 1533–1547.
[34] Z. Xiwang, N. Ziyao, D.K. Wang, J.C.D. da Costa, A novel ethanol dehydration process by forward osmosis, Chem. Eng. J. 232 (2013) 397–404.
[35] J.L. Braun, J.F. Kadla, Diffusion and saponification inside porous cellulose triacetate fibers, Biomacromolecules 6 (2005) 152–160.
[36] R.C. Ong, T.-S. Chung, Fabrication and positron annihilation spectroscopy (PAS) characterization of cellulose triacetate membranes for forward osmosis, J. Membr. Sci. 394–395 (2011) 230–240.
[37] Z. Sui, W.Y. KaiYu, T.-S. Chung, C. Hongmin, Y.C. Jean, G. Amy, Well-constructed cellulose acetate membranes for forward osmosis: Minimized internal concentration polarization with an ultra-thin selective layer, J. Membr. Sci. 360 (2010) 522–535.
[38] R. McGinnis, G. McGurgan, Forward osmosis membranes, US 8181794 B2, 2012.
[39] Z. Chunhua, Y. Fenglin, W. Wenjun, C. Bing, Preparation of PVA modified NWF and research of its antifouling performance, J. Chem. Eng. Chin. Univ. 22 (2008) 172–176.
[40] X. Zhikang, Y. Yang, Surface engineering of microporous polypropylene membranes, Membr. Sci. Technol. 9 (2008) 1775–1785.
[41] B. Xiaokai, L. Shi, G. Liang, L. Xiaofeng, Study of the preparation of PVA composite nanofiltration membrane, Membr. Sci. Technol. 24 (2004) 12–14.
[42] A. Tiraferri, N.Y. Yip, W.A. Phillip, J.D. Schiffman, M. Elimelech, Relating performance of thin-film composite forward osmosis membranes to support layer formation and structure, J. Membr. Sci. 367 (2011) 340–352.
[43] S. Loeb, L. Titelman, E. Korngold, J. Freiman, Effect of porous support fabric on osmosis through a Loeb-Sourirajan type asymmetric membrane, J. Membr. Sci. 129 (1997) 243–249.
[44] J.R. McCutcheon, M. Elimelech, Influence of concentrative and dilutive internal concentration polarization on flux behavior in forwardosmosis, J. Membr. Sci. 284 (2006) 237–247.
[45] X. Zhikang, W. Jianli, S. Liqiang, M. Dongfeng, X. Youyi, Microporous polypropylene hollow fiber membrane: Part 1. Surface modification by the graft polymerization of acrylic acid, J. Membr. Sci. 196 (2002) 221–229.